OPEN ACCESS
CellPress

Cell Reports
Report

Bicaudal D Family Adaptor Proteins Control the Velocity of Dynein-Based Movements

Max A. Schlager,[1,3] Andrea Serra-Marques,[2,3] Ilya Grigoriev,[2] Laura F. Gumy,[2] Marta Esteves da Silva,[2] Phebe S. Wulf,[2] Anna Akhmanova,[2,*] and Casper C. Hoogenraad[1,2,*]
[1]Department of Neuroscience, Erasmus Medical Center, Rotterdam, the Netherlands
[2]Cell Biology, Faculty of Science, Utrecht University, Utrecht, the Netherlands
[3]Co-first author
*Correspondence: a.akhmanova@uu.nl (A.A.), c.hoogenraad@uu.nl (C.C.H.)
http://dx.doi.org/10.1016/j.celrep.2014.07.052

SUMMARY

Cargo transport along microtubules is driven by the collective function of microtubule plus- and minus-end-directed motors (kinesins and dyneins). How the velocity of cargo transport is driven by opposing teams of motors is still poorly understood. Here, we combined inducible recruitment of motors and adaptors to Rab6 secretory vesicles with detailed tracking of vesicle movements to investigate how changes in the transport machinery affect vesicle motility. We find that the velocities of kinesin-based vesicle movements are slower and more homogeneous than those of dynein-based movements. We also find that Bicaudal D (BICD) adaptor proteins can regulate dynein-based vesicle motility. BICD-related protein 1 (BICDR-1) accelerates minus-end-directed vesicle movements and affects Rab6 vesicle distribution. These changes are accompanied by reduced axonal outgrowth in neurons, supporting their physiological importance. Our study suggests that adaptor proteins can modulate the velocity of dynein-based motility and thereby control the distribution of transport carriers.

INTRODUCTION

Intracellular transport allows cells to quickly and accurately direct a large variety of subcellular components to specific sites. Transport vesicles usually contain both kinesin and dynein motors and display typical back-and-forth movements along microtubules (MTs). The correct cellular distribution of cargos strongly depends on the balance of these bidirectional movements (Welte, 2010). An important question is, what determines the velocity of a cargo that is driven by motors of opposite polarity? One possibility is that the velocity directly reflects the number of engaged motors. However, results obtained by inferring the motor number from measurements of the forces that drive individual cargos do not support this hypothesis (Shubeita et al., 2008). The size of the cargo (and thus the drag it exerts), as well as additional motors present on the same cargo, might affect the velocity of its movement (Bieling et al., 2010; Erickson et al., 2011; Pan et al., 2006). Finally, various adaptor proteins and cofactors that link motors to cargo have been implicated in regulating cargo movement (Akhmanova and Hammer, 2010; Jolly and Gelfand, 2011; Schlager and Hoogenraad, 2009).

Cytoplasmic dynein is a versatile motor that is known to associate with a large number of adaptor proteins (Kardon and Vale, 2009), but the effect of these proteins on dynein properties, including the rate of translocation, is still poorly understood (Allan, 2011). A well-studied group of dynein adaptors is the evolutionarily conserved Bicaudal D (BICD) family. BICD is an essential factor in *Drosophila* oogenesis and embryogenesis that functions by controlling dynein-mediated mRNA transport (Bullock et al., 2006; Claussen and Suter, 2005). Mammals possess two BICD homologs, BICD1 and BICD2 (Hoogenraad et al., 2001; Matanis et al., 2002), as well as two more distantly related proteins named BICDR-1 and BICDR-2 (Schlager et al., 2010). Mammalian BICD family proteins have been implicated in Rab6 secretory vesicle trafficking (Grigoriev et al., 2007; Matanis et al., 2002) and nuclear positioning (Splinter et al., 2010). Recent studies identified various mutations in the human *BICD2* gene in patients with dominant congenital spinal muscular atrophy (Lipka et al., 2013).

Although they are primarily known as dynein adaptors, BICD family proteins have also been shown to bind to kinesins. BICD2 interacts with kinesin-1 (KIF5) family members, and BICDR-1 binds to kinesin-3 KIF1C (Grigoriev et al., 2007; Matanis et al., 2002). This suggests that BICD proteins play a complex regulatory role in cargo movement. In this study, we investigate this role using Rab6 vesicles as a model system. We show that BICD2 and BICDR-1 interact with dynein-dynactin through the same highly conserved domain and yet differentially affect Rab6 vesicle movement. We demonstrate that BICDR-1 strongly increases Rab6 vesicle speed in the MT minus-end direction and provide data indicating that the proper control of Rab6 vesicle trafficking is important for neuronal development.

RESULTS AND DISCUSSION

Kinesin Family Members Alter the Velocity of MT Plus-End-Directed Rab6 Vesicle Movements

The opposing MT-based motors dynein and kinesin have previously been implicated in Rab6 vesicle motility (Grigoriev et al.,

2007; Matanis et al., 2002; Schlager et al., 2010). Since several kinesins, including KIF5B and KIF1C, and cytoplasmic dynein bind to BICD family proteins (Grigoriev et al., 2007; Matanis et al., 2002; Schlager et al., 2010), and the activities of dynein and kinesin motors appear to be closely interlinked (Jolly and Gelfand, 2011), we first set out to determine the influence of kinesin motors on Rab6 transport. We used the FRB-FKBP dimerization system in combination with the cell-permeable rapamycin analog AP21967 (rapalog) to trigger binding of the dimeric motor domains (MDCs) of KIF5B or KIF1C to Rab6 vesicles (Figure 1A; Kapitein et al., 2010; Splinter et al., 2012) and investigated vesicle motility (Figure S1A). To distinguish the direction of Rab6 vesicle movements, we performed two-color imaging in MRC5-SV human lung fibroblasts in which the MT cytoskeleton is very sparse and can be easily visualized with mCherry-tagged α-tubulin (Figure 1B). In these conditions, MT plus ends can be distinguished by the presence of growth episodes, allowing identification of the direction of Rab6 vesicle movement (Splinter et al., 2012). We found that rapalog-induced KIF5B-MDC recruitment to Rab6 vesicles (Figures 1C and S1B–S1D) significantly decreased the mean speed of Rab6 vesicles in the MT plus-end direction, from ~1.7 μm/s to ~1.3 μm/s, and consequently the percentage of rapid events (Figures 1D and 1F). Conversely, KIF1C-MDC recruitment increased the velocity of Rab6 vesicles toward the MT plus ends to ~2.0 μm/s, and in this case the proportion of events that displayed high speed was higher (Figures 1D and 1F). These data show that the recruitment of distinct kinesins can differentially modulate MT plus-end-directed vesicle velocity. Interestingly, recruitment of either kinesin resulted in a marked narrowing of the velocity distribution profiles (Figure 1D), as was apparent from their reduced variances (Figure 1E). In contrast, recruitment of the rigor mutant KIF5B-MDC-T92N (Nakata and Hirokawa, 1995) arrests Rab6 vesicles on MTs (Movie S1; Figure S1E), showing that the results we observe are due to the recruitment of a kinesin with specific properties to the vesicles. Altogether, these results suggest that when the population of motors on the vesicles becomes more homogeneous, because of recruitment of an excess of one particular motor, the velocities of movement become more homogeneous as well. We conclude that it is the nature of the motors, rather than their number, that determines vesicle velocity.

In spite of the significant changes in Rab6 vesicle velocities in the MT plus-end direction, the velocity of minus-end-directed movement (~2.4 μm/s, ~1.5 times higher than the velocity of plus-end-directed movements) was largely unaffected by kinesin tethering to Rab6 vesicles (Figures 1D–1F). Thus, an increase in the number of kinesin motors on the Rab6 cargo had no major consequences for the velocity of dynein-dependent motility. These data are in line with the view that opposite-polarity motors on the same cargo do not directly affect each other's motility, but rather alter the number of runs occurring in each direction (Kapitein et al., 2010; Splinter et al., 2012; Xu et al., 2012). However, we cannot exclude the possibility that endogenous full-length motors bound to cargos by their native linkage mechanisms behave differently from the truncated motors used in the inducible trafficking assay.

Dynein Drives Rapid Rab6 Vesicle Movements

To analyze in more detail the effect of different MT-based motors on Rab6 vesicle velocity, we performed small interfering RNA (siRNA)-mediated depletion of KIF5B, KIF1C, KIF1B (the close homolog of KIF1C), dynein heavy chain (DHC), and combinations thereof. The depletion efficiency was ~70%–90% (Figures S2A–S2C). We performed the experiments in HeLa cells because we were not able to achieve efficient knockdown in MRC5-SV cells. Due to the extremely high density of the MT system in HeLa cells, we could not unambiguously trace individual vesicles along individual MTs. Therefore, MT plus-end- and minus-end-directed runs were analyzed together. Using maximum intensity projections, we identified episodes of vesicle motility and measured their velocities (Figures S1A and S2D). None of the analyzed motor depletions led to a complete inhibition of the overall transport of Rab6 vesicles from the Golgi to the cell periphery (Figures S2D and S2E). The knockdown of single kinesin proteins caused a mild increase in the mean velocity of Rab6 vesicles to ~1.7 μm/s (Figures S2D and S2E). Simultaneous depletion of all three kinesins resulted in a stronger effect (mean velocity of ~2.2 μm/s; Figures S2D and S2E).

We next tested the contribution of dynein to Rab6 vesicle movement. Depletion of DHC decreased the average velocity of vesicle movement to ~1.2 μm/s (Figures S2D and S2E) and reversed the effect of kinesin depletion (Figures S2D–S2F). These data strongly suggest that the rapid Rab6 vesicle movements are dynein-based, which is consistent with the observation that rapid Rab6 movements in MRC5-SV cells are predominantly MT minus-end-directed (Figures 1D, S2D, and S2E). When kinesins were depleted, rapid dynein movements started to predominate, increasing the average speed of Rab6 vesicles, whereas the depletion of dynein led to a relatively larger proportion of the slower kinesin-driven movements. It is also interesting to point out that velocities of dynein-based Rab6 vesicle movements display much broader distribution profiles (higher variance) than the kinesin-driven ones (Figures S2D and S2E). This heterogeneity might be due to the fact that dynein requires multiple adaptors and regulatory factors for its motility (Allan, 2011; Kardon and Vale, 2009).

BICD2 and BICDR-1 Interact with Dynein and Dynactin in a Similar Fashion

To explore the role of adaptor proteins in regulating dynein-driven cargo movement, we focused on the BICD family of proteins. Since both BICD2 and BICDR-1 interact with the dynein complex (Grigoriev et al., 2007; Matanis et al., 2002; Schlager et al., 2010) and colocalize with dynein on vesicles (Figures 2A and 2B; Movies S2 and S3), we first set out to compare the interactions of two BICD family members with the dynein complex in more detail. We performed immunoprecipitation experiments with extracts of HeLa cells stably expressing GFP-tagged DHC (Poser et al., 2008). Apart from some minor experimental variations, DHC consistently coprecipitated both BICD2 and BICDR-1 in equal amounts (Figure 2C). We confirmed this observation by additional immunoprecipitation experiments using antibodies specific for the endogenous dynein intermediate chain (DIC) (Figure 2D). Taken together, these results suggest

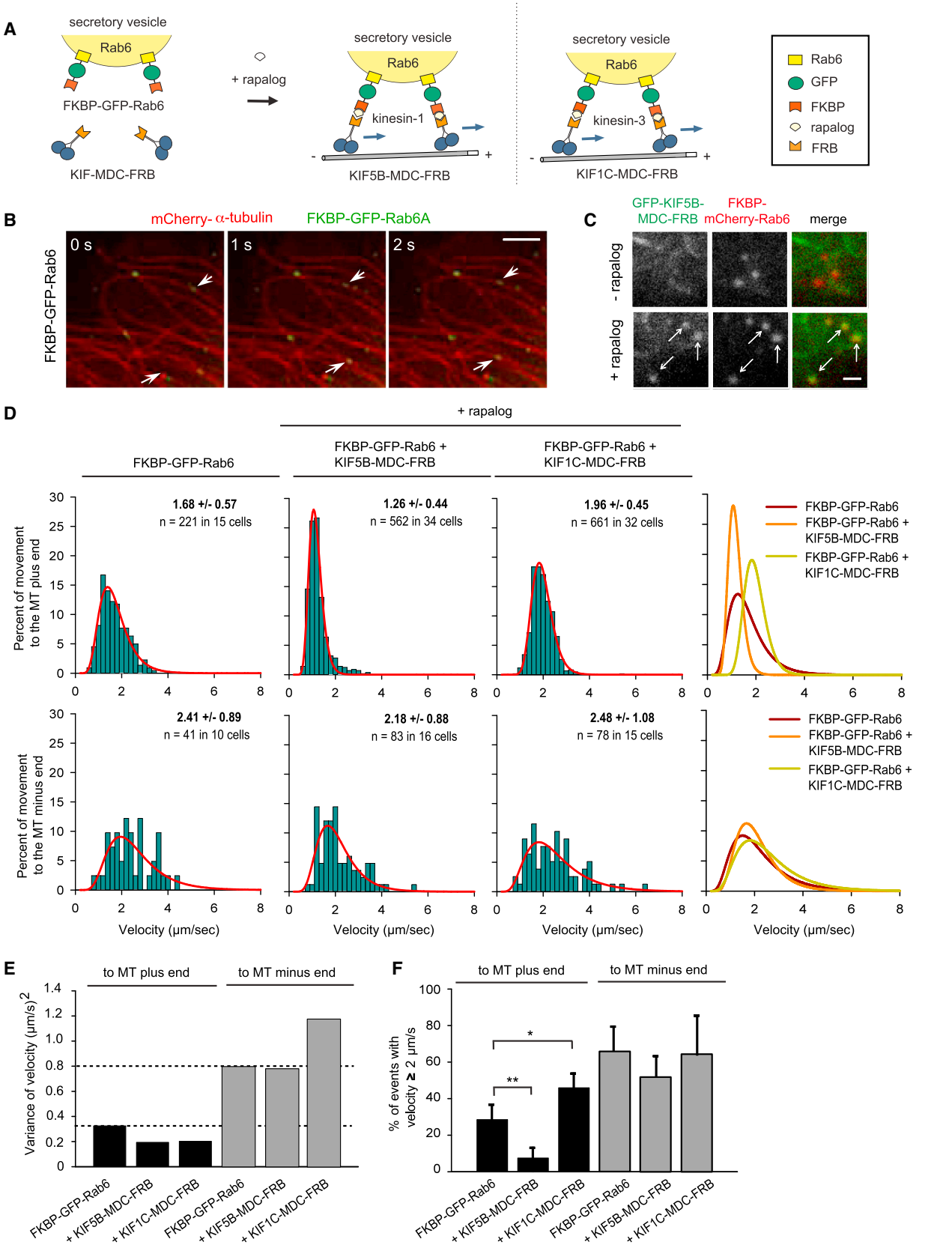

(legend on next page)

that BICD2 and BICDR-1 interact with the dynein motor equally well.

Next, we set out to map the dynein interaction site of BICD2 and BICDR-1 proteins more precisely. Various members of the BICD protein family are very similar in structure: they are coiled coil proteins with a cargo-binding site located in the C terminus and motor-binding sites in the N-terminal half of the molecule (Hoogenraad et al., 2001, 2003; Liu et al., 2013; Schlager et al., 2010; Splinter et al., 2012). By comparing the amino acid sequences of *Drosophila* and mouse BICD family members, we found a highly conserved region in the N terminus of these proteins (Figures 2E and S3). This domain shows homology to the HAP1_N conserved region (Pfam protein database: *pf04849*) and could be involved in the interaction with dynein and dynactin (Hoogenraad et al., 2001, 2003). Interestingly, a conserved alanine residue present in the center of this region is substituted by valine in the *Drosophila* hypomorphic mutant $BicD^{PA66}$ (Oh et al., 2000) and is conserved in BICD family members and other adaptor proteins, such as HAP1 and TRAK1/2. Adjacent to this conserved alanine, mouse BICD family members have an additional alanine residue (Figure 2E). We hypothesized that the mutation of these alanine residues might affect the interaction of BICD family members with the dynein-dynactin complex. To test this, we generated BICD2 and BICDR-1 mutants, BICD2-A43V-A44V (BICD2-A/V) and BICDR-1-A116V-A117V (BICDR-1-A/V), respectively (Figure 2E). We found that the amount of A/V mutant BICD2 and BICDR-1 that coprecipitated with the dynein complex was dramatically reduced compared with the wild-type proteins (Figure 2F). This result was confirmed by a reverse immunoprecipitation (Figures 2G and 2H), indicating that the A/V mutations interfere with the ability of both BICD2 and BICDR-1 to bind to dynein and dynactin. These data show that BICD2 and BICDR-1 interact with dynein and dynactin through the same conserved N-terminal domain.

Despite the strong similarities between BICD2 and BICDR-1 in biochemical assays, their cellular distribution is markedly distinct (Schlager et al., 2010). HeLa cells expressing BICD2 showed a diffuse staining pattern with a small accumulation around the centrosome, whereas BICDR-1 showed a strong pericentrosomal accumulation (Figure 2I). Consistent with the biochemical data, the intensity of the A/V mutants at the pericentrosomal region was strongly reduced (Figures 2I and 2J). Together, these results demonstrate that the mutation of these alanine residues affects the interaction of BicD proteins with the dynein-dynactin complex.

BICD Adaptors Control the Velocity of Dynein-Based Movements

BICD2 and BICDR-1 expression also differentially affected the Rab6 vesicle distribution in HeLa cells (Figures 3A and 3B). Whereas overexpression of BICD2 only resulted in a very small recruitment of endogenous Rab6 vesicles to the centrosome, expression of BICDR-1 caused a strong pericentrosomal accumulation of Rab6 vesicles (Figures 3A and 3B). To directly test the effect of BICD proteins on Rab6 vesicle motility, we transiently expressed either BICD2 or BICDR-1 in HeLa cells stably expressing GFP-Rab6 and analyzed the movement of Rab6 vesicles. The expression of BICD2 increased the mean Rab6 vesicle velocity from ~1.5 μm/s to ~1.9 μm/s, while BICDR-1 caused a much larger increase, to ~3.3 μm/s (Figures 3C and 3G; Movie S4). Kymograph analysis of individual vesicle tracks revealed that the increase in velocity was not caused by altered motor switching, but was mainly due to the fact that long processive runs occurred with a higher speed (Figures 3D and 3F). The BICDR-1-induced increase in Rab6 vesicle velocity was also observed in several other cell types, including MRC5-SV and Vero cells (Figure 3E). We next tested the contribution of dynein to the BICDR-1-mediated increase in Rab6 vesicle velocity. Depletion of DHC in BICDR-1-expressing HeLa cells decreased the number of motile Rab6 vesicles and reduced the average velocity from 3.3 μm/s to 2.0 μm/s (Figure 3I). Moreover, expression of the BICDR-1 A/V mutant showed decreased Rab6 vesicle motility compared with BICDR-1 wild-type (Figures S4A and S4B). These data indicate that the BICDR-1-induced increase in Rab6 vesicle motility is dynein based, which is consistent with the BICDR-1-mediated accumulation of Rab6 in the pericentrosomal region (Figures 3A and 3B).

To further prove that the increase in vesicle velocity induced by BICDR-1 expression is due to modulation of dynein motility, we switched back to MRC5-SV expressing mCherry-α-tubulin. Quantitative single-particle tracking revealed that BICDR-1 expression markedly increased the mean Rab6 vesicle speed in the MT minus-end direction, from ~2.3 μm/s to ~3.6 μm/s (Figure 3H). The velocity of plus-end-directed movements was also increased from ~1.6 μm/s in control cells to ~2.2 μm/s (Figure 3H). This could be caused by a change in the set of vesicle-associated kinesin motors, for example, by the enhanced recruitment of a more rapid kinesin such as KIF1C, which is known to interact with BICDR-1 (Schlager et al., 2010). These data demonstrate that BICDR-1 induces a strong increase in Rab6 vesicle velocity, predominantly in the MT minus-end direction.

Figure 1. Distinct Kinesin Motors Differentially Alter Rab6 Vesicle Motility

(A) Inducible Rab6 secretory-vesicle trafficking assay. Fusions of FRB with the motor domain and coiled-coil dimerization region of kinesin-1 (KIF5-MDC-FRB) and kinesin-3 (KIF1C-MDC-FRB) are recruited to FKBP-GFP-Rab6 upon addition of rapalog.

(B) Simultaneous live imaging of FKBP-GFP-Rab6 vesicles (green, arrows) and mCherry-α-tubulin (red) in a transiently transfected MRC5-SV cell; time is indicated in seconds. Imaging of FKBP-GFP-Rab6 in MRC5-SV cells expressing HA-KIF5B-T92N-MDC-FRB is shown in Movie S1. Scale bar, 3 μm.

(C) Representative stills of a small region of a cell transfected with GFP-KIF5B-MDC-FRB and FKBP-mCherry-Rab6 before (–) and after (+) rapalog addition. Arrows indicate Rab6 vesicles. Images are related to Figures S1B–S1D. Scale bar, 1 μm.

(D) Analysis of Rab6 vesicle movement along MTs within the cell upon rapalog-induced recruitment of either KIF5-MDC-FRB or KIF1C-MDC-FRB.

(E) Variance in velocity of Rab6 vesicle movements toward either the MT plus or minus end upon recruitment of the indicated motor constructs.

(F) Percentage of Rab6 vesicle movement events in the direction of either the MT plus or minus end with a velocity of ≥2 μm/s (average ± SD). *$p < 0.01$, **$p < 0.001$, Mann-Whitney U test.

See also Figure S2.

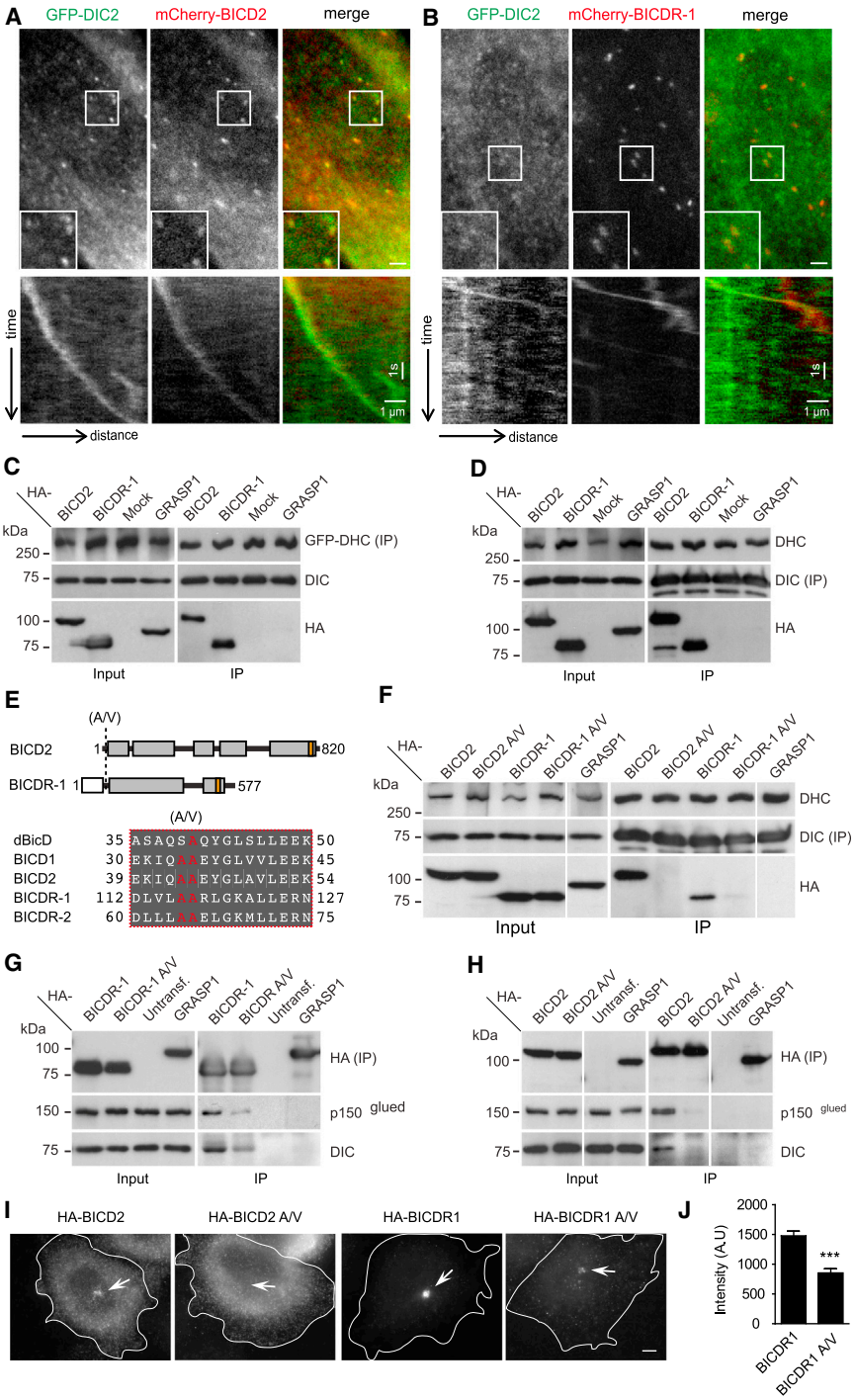

Figure 2. Identification of the Conserved Binding Site for Dynein-Dynactin in the N Terminus of BICD Family Proteins

(A and B) HeLa cells stably expressing GFP-DIC2 were transfected with mCherry-BICD2 (A) or mCherry-BICDR-1 (B). The images correspond to one frame of Movies S2 and S3. Kymographs are shown to illustrate the movement of vesicles labeled with GFP-DIC2 and the indicated transfected constructs. Scale bars, 2 µm.

(C) Immunoprecipitations with anti-GFP antibodies from extracts of HeLa cells stably expressing GFP-DHC, transfected with the indicated constructs and probed for DHC, DIC, or hemagglutinin (HA).

(D) Immunoprecipitations with antibodies against DIC from extracts of HeLa cells transfected with the indicated constructs and probed for DHC, DIC, or HA.

(E) Schematic overview of BICD2/BICDR-1 and a section of a sequence alignment of *Drosophila* BicD (dBicD, NP_724056.1), mouse BICD1 (NP_033883), BICD2 (NP_084067), BICDR-1 (NP_001074277), and BICDR-2 (NP_722479). The dashed red line and red letters indicate the site of the dBicD-A40V (*BicD*^{PA66}), BICD2-A116V-A117V (BICD2 A/V), and BICDR-1-A43V-A44V (BICDR-1 A/V) mutations.

(F) Immunoprecipitations with antibodies against DIC from extracts of HeLa cells transfected with the indicated constructs and probed for DHC, DIC, or HA.

(G) Immunoprecipitations with anti-HA antibodies from extracts of HeLa cells transfected with the indicated constructs and probed for DIC, p150Glued, or HA.

(H) Immunoprecipitations with anti-HA antibodies from extracts of HeLa cells transfected with the indicated constructs and probed for DIC, p150Glued, or HA.

(I) Representative image of a HeLa cell overexpressing HA-BICD2, HA-BICD2 A/V, HA-BICDR-1 A/V, or HA-BICDR-1 stained for HA. Solid lines indicate the cell edge, and arrows indicate the centrosome region. Scale bar, 5 µm.

(J) Quantification of the intensity of HA-BICDR-1 and HA-BICDR-1 A/V signal at the centrosome (average ± SEM; HA-BICDR-1, n = 41 cells; HA-BICDR-1 A/V, n = 45 cells; n = 2 independent experiments). ***p < 0.0001, t test.

See also Figure S3.

BICD Adaptors Control the Distribution of Rab6 Vesicles and Axonal Outgrowth

BICDR-1 is primarily found in the brain, is expressed in hippocampal and dorsal root ganglion (DRG) neurons, and is required for neural development in zebrafish (Schlager et al., 2010). To test its cellular effect in neuronal systems, we transiently expressed BICD2 and BICDR-1 in developing hippocampal and adult DRG neurons and analyzed the Rab6 vesicle distribution. BICD2 did not affect the distribution of Rab6 vesicles in the neuronal cell body and axons (Figures 4A and 4C). In contrast, BICDR-1 expression induced a strong accumulation of Rab6 vesicles in the cell bodies and led to a ~3-fold decrease in the number of axonal Rab6 vesicles Figures 4A–4D). Interestingly, BICDR-1 expression in hippocampal and DRG neurons showed a marked reduction in axon outgrowth compared with control cells (Figures 4E–4H). The total axon length was decreased by ~50% in BICDR-1 expressing neurons, but no difference was observed in GFP-BICD2- or GFP-expressing neurons (Figures 4F and 4H). These results

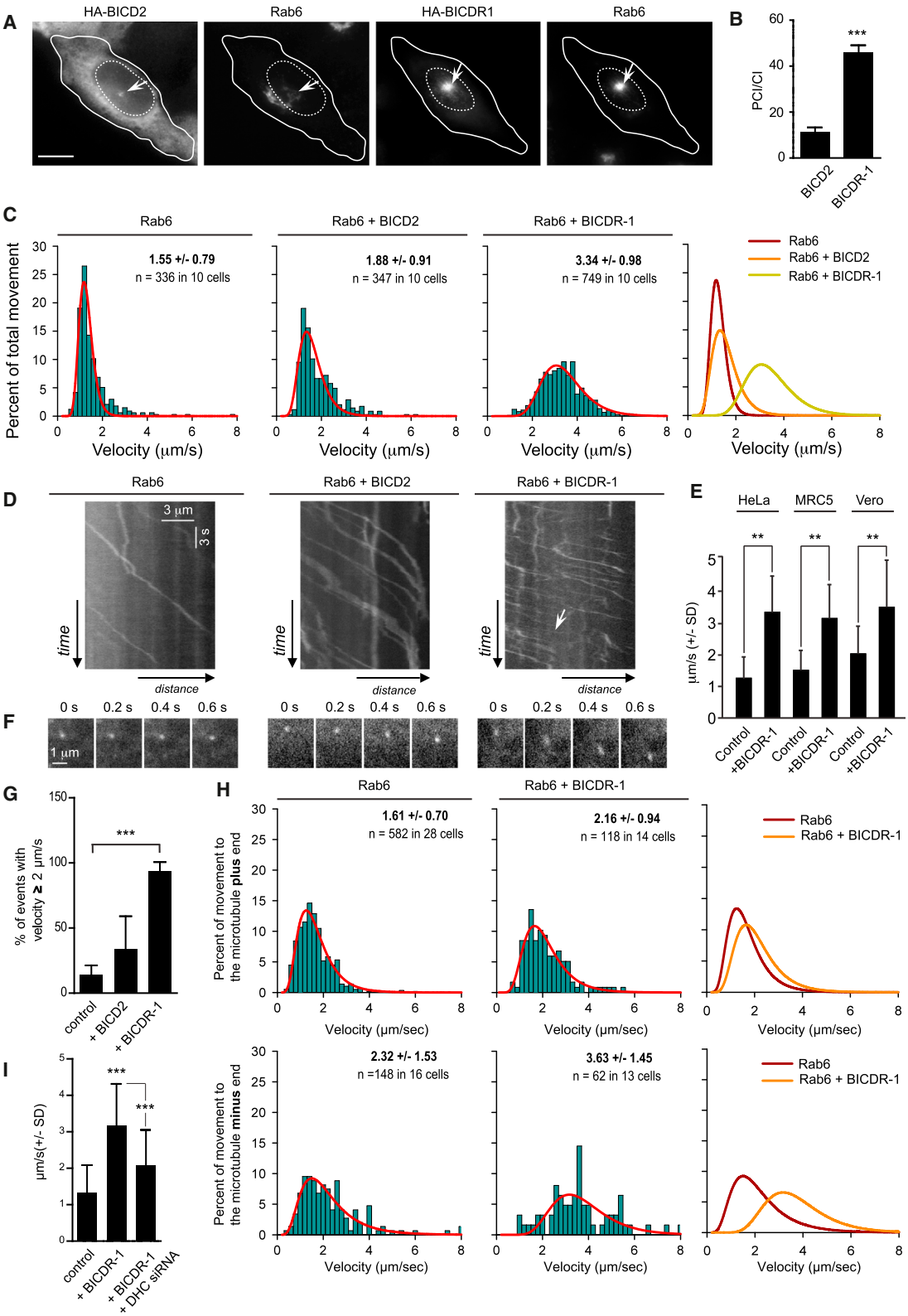

Figure 3. BICDR-1 Increases Rab6 Vesicle Velocity in the MT Minus-End Direction

(A) Representative image of a HeLa cell overexpressing HA-BICD2 or HA-BICDR-1, stained for HA and endogenous Rab6. Solid lines indicate the cell edge, dashed lines indicate the nucleus, and arrows indicate the centrosome region. Scale bar, 10 μm.

(legend continued on next page)

suggest that the observed axon phenotype is due to BICDR-1-induced loss of Rab6 secretory vesicles from the neurites. In agreement with this interpretation, DRG neurons transfected with both Rab6A- and Rab6B-shRNA showed a 50% reduction of total axon length compared with control cells and single Rab6A- or Rab6B-depleted neurons (Figures 4I and 4J), suggesting that Rab6A and Rab6B have an important function in axon outgrowth. These data are consistent with previous results obtained in hippocampal neurons (Schlager et al., 2010) and show that BICDR-1 influences Rab6 vesicle distribution, an effect that is accompanied by altered axonal elongation in both young and adult neurons.

It is interesting to speculate about the possible molecular mechanisms that underlie the observed differences between BICDR-1 and BICD2. One possibility is that the two adaptors interact with different kinesins, which would differentially influence dynein-dependent movements. However, the depletion of various kinesin combinations in BICD2-overexpression did not increase vesicle velocities to the levels observed with BICDR-1 expression (Figures S4C–S4F). Another possibility is that BICDR-1 recruits higher-order assemblies of dynein-dynactin to Rab6 vesicles compared with BICD2, thereby leading to the observed increase in Rab6 vesicle velocity. In vitro studies have shown that changing the number of dynein motors allows robust dynein-driven motion (Derr et al., 2012; Mallik et al., 2005). Moreover, increased minus-end-directed transport of cytoplasmic mRNA in *Drosophila* embryos has been reported to depend on the dosage of BICD and dynein motors (Bullock et al., 2006). Nevertheless, it seems unlikely that the increase in Rab6 vesicle velocity is caused by the enhanced recruitment of dynein-dynactin to Rab6 vesicles, since both BICD2 and BICDR-1 precipitated dynein and dynactin equally well and the interaction could be disrupted by the mutation of the same protein domain. Furthermore, direct imaging of GFP-tagged dynein provided no clear indications of enhanced recruitment by BICDR-1 as compared with BICD2 (Figures 2A and 2B).

One other possibility is that BICDR-1 directly regulates the dynein-dynactin complex and enhances dynein motor activity. Several recent results point to a regulatory mechanism whereby alterations in the dynein tail influence the motor domains (Vallee et al., 2012). In vitro work has shown that dynein cofactors such as Lis1 and NudE can alter the properties of dynein, including its mechanochemical cycle and processivity (Huang et al., 2012; McKenney et al., 2010). The idea that multiple adaptors and regulatory factors are involved in controlling dynein-based motility is consistent with the broad minus-end-directed velocity distribution profiles. However, the mechanistic details underlying the contributions of different adaptors and accessory factors to dynein motor velocity remain an unresolved issue that requires future work.

EXPERIMENTAL PROCEDURES

DNA Constructs, siRNAs, and Cell Lines

Details regarding the BICD2, BICDR-1, Rab6, kinesin constructs, and siRNAs used in this work are provided in Supplemental Experimental Procedures. The HeLa cell lines stably expressing GFP-DIC2 and GFP-DHC were a gift from Dr. Anthony Hyman.

Primary Hippocampal Neuron and DRG Neuron Cultures

Primary hippocampal cultures were prepared from embryonic day 18 (E18) rat brains and transfected using Lipofectamine 2000 (Invitrogen). DRG neurons were isolated from adult female Sprague Dawley rats (3 months old) and transfected using a Microporator (Invitrogen). For details, see Supplemental Experimental Procedures.

Image Acquisition and Live-Cell Imaging

Images of fixed cells were collected with a Leica DMRBE microscope equipped with an ORCA-ER-1394 CCD camera (Hamamatsu) or Nikon Eclipse 80i microscope equipped with a Photometrics CoolSNAP HQ2 CCD camera. Live-cell imaging was performed on a total internal reflection fluorescence inverted research microscope (Nikon Eclipse Ti-E; Nikon) at 37°C in standard culture medium in a closed chamber with 5% CO_2 (Tokai Hit). For details, see Supplemental Experimental Procedures.

SUPPLEMENTAL INFORMATION

Supplemental Information includes Supplemental Experimental Procedures, four figures, and four movies and can be found with this article online at http://dx.doi.org/10.1016/j.celrep.2014.07.052.

AUTHOR CONTRIBUTIONS

M.A.S. cloned the DNA constructs, designed and performed biochemical experiments, and edited the manuscript. A.S.-M. designed and performed knockdown and imaging experiments, analyzed the results, and edited the manuscript. I.G. performed imaging experiments and analyzed the results. L.F.G. performed the DRG neuron experiments and analyzed the results. M.E.d.S. performed the hippocampal neuron experiments and analyzed the results. P.S.W. assisted with cloning the DNA constructs. A.A. and C.C.H. supervised the research and wrote the manuscript.

(B) Ratio of pericentrosomal (PCI) versus cytoplasmic (CI) Rab6 fluorescence intensity in cells overexpressing either HA-BICD2 or HA-BICDR-1 (average ± SEM; HA-BICD2, n = 44; HA-BICDR-1, n = 41 cells). ***$p < 0.0001$, Mann-Whitney test.
(C) Histograms of Rab6 vesicle speeds in HeLa cells stably expressing GFP-Rab6 and transfected for the indicated constructs. GFP-Rab6 motility in HeLa cells in the absence or presence of BICDR-1 is shown in Movie S4.
(D) Kymographs illustrating the movements of GFP-Rab6 vesicles in untransfected cells or cells transfected with the indicated constructs. Scale bar, 3 μm.
(E) Average speed (± SD) of GFP-Rab6 vesicles toward the cell center in HeLa, MRC5-SV, or Vero cells transfected with either a control construct or BICDR-1. **$p < 0.001$, Mann-Whitney U test.
(F) Time-lapse images of GFP-Rab6 vesicles in HeLa cells transfected with either BICD2 or BICDR-1. Time is in seconds.
(G) Overexpression of BICD2 and BICDR-1 led to an increase in the percentage of Rab6 vesicle movement ≥ 2 μm/s (average ± SD). ***$p < 0.001$, unpaired t test.
(H) Histograms of vesicle speeds toward the MT plus or minus end in MRC5-SV cells transfected with GFP-Rab6A and BICDR-1 when indicated. The indicated values correspond to mean ± SD.
(I) Average speed (± SD) of GFP-Rab6 vesicles in HeLa transfected with a control construct, BICDR-1, or BICDR-1 and DHC siRNA. ***$p < 0.0001$, Mann-Whitney U test.
See also Figure S4.

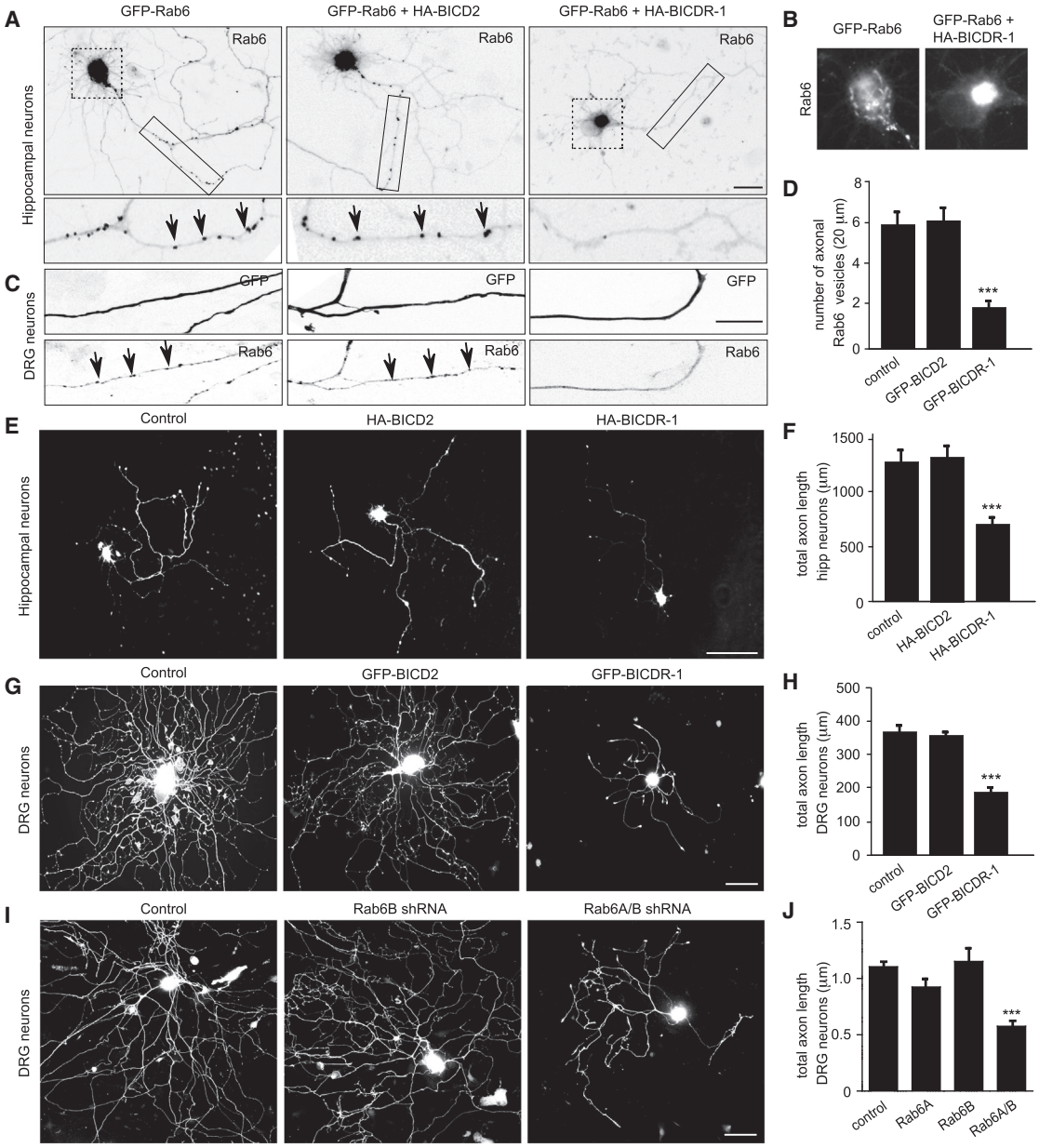

Figure 4. Proper Rab6 Vesicle Distribution Is Important for Axon Elongation in Neurons

(A) Representative images of hippocampal neurons expressing GFP-Rab6, HA-BICD2, or HA-BICDR-1. Scale bar, 20 μm. Enlarged boxed areas correspond to a region of the axon and arrows indicate Rab6 vesicles.

(B) Enlargement of the cell body of the neurons presented in (A) (dashed-line boxes).

(C) Representative images of axons of DRG neurons expressing GFP to highlight neuronal morphology, TagRFP-Rab6, and HA-BICD2 or HA-BICDR-1. Arrows indicate Rab6 vesicles. Scale bar, 10 μm.

(D) Quantification of the number of TagRFP-Rab6 vesicles in axons of DRG neurons transfected with the indicated constructs. Error bars indicate SEM. ***$p < 0.001$, t test.

(E and G) Representative images of hippocampal neurons at 4 days in vitro (DIV4) and DRG neurons at DIV2 transfected with TagBFP and the indicated constructs. Scale bar, 100 μm.

(F and H) Quantification of axon length in TagBFP (control) and HA-BICD2 or HA-BICDR-1 cotransfected hippocampal neurons (DIV4; n = 31–37 cells, n = 3 independent experiments) or GFP (control), GFP-BICDR-1, and GFP-BICD2 transfected DRG neurons (DIV1; n = 53–87 cells; n = 3 independent experiments). Error bars indicate SEM. ***$p < 0.001$, t test.

(I) Representative images of DRG neurons (DIV4) transfected with GFP and the indicated constructs. Scale bar, 100 μm.

(J) Quantification of axon length in GFP and pSuper (control), Rab6A-shRNA, Rab6B-shRNA, or Rab6A/B-shRNA cotransfected DRG neurons (DIV4; n = 31–40 cells; n = 3 independent experiments). Error bars indicate SEM. ***$p < 0.001$, t test.

ACKNOWLEDGMENTS

We thank Drs. Ina Poser and Anthony Hyman for sharing HeLa cells stably expressing GFP-tagged DHC and DIC2. This work was supported by Fundação para a Ciência e a Tecnologia fellowships (A.S.-M. and M.E.S.), the Netherlands Organization for Scientific Research (NWO-ALW-VICI; A.A. and C.C.H.), the Netherlands Organization for Health Research and Development (ZonMW-TOP; A.A. and C.C.H.), the European Science Foundation (EURYI; C.C.H.), the EMBO Young Investigators Program (YIP; C.C.H.), the Research Programme of the Foundation for Fundamental Research on Matter (FOM; A.A. and C.C.H.), a Het Prinses Beatrix Spierfonds grant (PBF; C.C.H.), and an FP7 EU Marie Curie postdoctoral fellowship (L.F.G.).

Received: April 10, 2013
Revised: June 8, 2014
Accepted: July 28, 2014
Published: August 28, 2014

REFERENCES

Akhmanova, A., and Hammer, J.A., 3rd. (2010). Linking molecular motors to membrane cargo. Curr. Opin. Cell Biol. *22*, 479–487.

Allan, V.J. (2011). Cytoplasmic dynein. Biochem. Soc. Trans. *39*, 1169–1178.

Bieling, P., Kronja, I., and Surrey, T. (2010). Microtubule motility on reconstituted meiotic chromatin. Curr. Biol. *20*, 763–769.

Bullock, S.L., Nicol, A., Gross, S.P., and Zicha, D. (2006). Guidance of bidirectional motor complexes by mRNA cargoes through control of dynein number and activity. Curr. Biol. *16*, 1447–1452.

Claussen, M., and Suter, B. (2005). BicD-dependent localization processes: from Drosophilia development to human cell biology. Ann. Anat. *187*, 539–553.

Derr, N.D., Goodman, B.S., Jungmann, R., Leschziner, A.E., Shih, W.M., and Reck-Peterson, S.L. (2012). Tug-of-war in motor protein ensembles revealed with a programmable DNA origami scaffold. Science *338*, 662–665.

Erickson, R.P., Jia, Z., Gross, S.P., and Yu, C.C. (2011). How molecular motors are arranged on a cargo is important for vesicular transport. PLoS Comput. Biol. *7*, e1002032.

Grigoriev, I., Splinter, D., Keijzer, N., Wulf, P.S., Demmers, J., Ohtsuka, T., Modesti, M., Maly, I.V., Grosveld, F., Hoogenraad, C.C., and Akhmanova, A. (2007). Rab6 regulates transport and targeting of exocytotic carriers. Dev. Cell *13*, 305–314.

Hoogenraad, C.C., Akhmanova, A., Howell, S.A., Dortland, B.R., De Zeeuw, C.I., Willemsen, R., Visser, P., Grosveld, F., and Galjart, N. (2001). Mammalian Golgi-associated Bicaudal-D2 functions in the dynein-dynactin pathway by interacting with these complexes. EMBO J. *20*, 4041–4054.

Hoogenraad, C.C., Wulf, P., Schiefermeier, N., Stepanova, T., Galjart, N., Small, J.V., Grosveld, F., de Zeeuw, C.I., and Akhmanova, A. (2003). Bicaudal D induces selective dynein-mediated microtubule minus end-directed transport. EMBO J. *22*, 6004–6015.

Huang, J., Roberts, A.J., Leschziner, A.E., and Reck-Peterson, S.L. (2012). Lis1 acts as a "clutch" between the ATPase and microtubule-binding domains of the dynein motor. Cell *150*, 975–986.

Jolly, A.L., and Gelfand, V.I. (2011). Bidirectional intracellular transport: utility and mechanism. Biochem. Soc. Trans. *39*, 1126–1130.

Kapitein, L.C., Schlager, M.A., van der Zwan, W.A., Wulf, P.S., Keijzer, N., and Hoogenraad, C.C. (2010). Probing intracellular motor protein activity using an inducible cargo trafficking assay. Biophys. J. *99*, 2143–2152.

Kardon, J.R., and Vale, R.D. (2009). Regulators of the cytoplasmic dynein motor. Nat. Rev. Mol. Cell Biol. *10*, 854–865.

Lipka, J., Kuijpers, M., Jaworski, J., and Hoogenraad, C.C. (2013). Mutations in cytoplasmic dynein and its regulators cause malformations of cortical development and neurodegenerative diseases. Biochem. Soc. Trans. *41*, 1605–1612.

Liu, Y., Salter, H.K., Holding, A.N., Johnson, C.M., Stephens, E., Lukavsky, P.J., Walshaw, J., and Bullock, S.L. (2013). Bicaudal-D uses a parallel, homodimeric coiled coil with heterotypic registry to coordinate recruitment of cargos to dynein. Genes Dev. *27*, 1233–1246.

Mallik, R., Petrov, D., Lex, S.A., King, S.J., and Gross, S.P. (2005). Building complexity: an in vitro study of cytoplasmic dynein with in vivo implications. Curr. Biol. *15*, 2075–2085.

Matanis, T., Akhmanova, A., Wulf, P., Del Nery, E., Weide, T., Stepanova, T., Galjart, N., Grosveld, F., Goud, B., De Zeeuw, C.I., et al. (2002). Bicaudal-D regulates COPI-independent Golgi-ER transport by recruiting the dynein-dynactin motor complex. Nat. Cell Biol. *4*, 986–992.

McKenney, R.J., Vershinin, M., Kunwar, A., Vallee, R.B., and Gross, S.P. (2010). LIS1 and NudE induce a persistent dynein force-producing state. Cell *141*, 304–314.

Nakata, T., and Hirokawa, N. (1995). Point mutation of adenosine triphosphate-binding motif generated rigor kinesin that selectively blocks anterograde lysosome membrane transport. J. Cell Biol. *131*, 1039–1053.

Oh, J., Baksa, K., and Steward, R. (2000). Functional domains of the Drosophila bicaudal-D protein. Genetics *154*, 713–724.

Pan, X., Ou, G., Civelekoglu-Scholey, G., Blacque, O.E., Endres, N.F., Tao, L., Mogilner, A., Leroux, M.R., Vale, R.D., and Scholey, J.M. (2006). Mechanism of transport of IFT particles in C. elegans cilia by the concerted action of kinesin-II and OSM-3 motors. J. Cell Biol. *174*, 1035–1045.

Poser, I., Sarov, M., Hutchins, J.R., Hériché, J.K., Toyoda, Y., Pozniakovsky, A., Weigl, D., Nitzsche, A., Hegemann, B., Bird, A.W., et al. (2008). BAC TransgeneOmics: a high-throughput method for exploration of protein function in mammals. Nat. Methods *5*, 409–415.

Schlager, M.A., and Hoogenraad, C.C. (2009). Basic mechanisms for recognition and transport of synaptic cargos. Mol. Brain *2*, 25.

Schlager, M.A., Kapitein, L.C., Grigoriev, I., Burzynski, G.M., Wulf, P.S., Keijzer, N., de Graaff, E., Fukuda, M., Shepherd, I.T., Akhmanova, A., and Hoogenraad, C.C. (2010). Pericentrosomal targeting of Rab6 secretory vesicles by Bicaudal-D-related protein 1 (BICDR-1) regulates neuritogenesis. EMBO J. *29*, 1637–1651.

Shubeita, G.T., Tran, S.L., Xu, J., Vershinin, M., Cermelli, S., Cotton, S.L., Welte, M.A., and Gross, S.P. (2008). Consequences of motor copy number on the intracellular transport of kinesin-1-driven lipid droplets. Cell *135*, 1098–1107.

Splinter, D., Tanenbaum, M.E., Lindqvist, A., Jaarsma, D., Flotho, A., Yu, K.L., Grigoriev, I., Engelsma, D., Haasdijk, E.D., Keijzer, N., et al. (2010). Bicaudal D2, dynein, and kinesin-1 associate with nuclear pore complexes and regulate centrosome and nuclear positioning during mitotic entry. PLoS Biol. *8*, e1000350.

Splinter, D., Razafsky, D.S., Schlager, M.A., Serra-Marques, A., Grigoriev, I., Demmers, J., Keijzer, N., Jiang, K., Poser, I., Hyman, A.A., et al. (2012). BICD2, dynactin, and LIS1 cooperate in regulating dynein recruitment to cellular structures. Mol. Biol. Cell *23*, 4226–4241.

Vallee, R.B., McKenney, R.J., and Ori-McKenney, K.M. (2012). Multiple modes of cytoplasmic dynein regulation. Nat. Cell Biol. *14*, 224–230.

Welte, M.A. (2010). Bidirectional transport: matchmaking for motors. Curr. Biol. *20*, R410–R413.

Xu, J., Shu, Z., King, S.J., and Gross, S.P. (2012). Tuning multiple motor travel via single motor velocity. Traffic *13*, 1198–1205.